AIAA JOURNAL
Vol. 41, No. 7, July 2003

Properties of Particle-Generated Turbulence in the Final-Decay Period

K. Lee* and G. M. Faeth†
University of Michigan, Ann Arbor, Michigan 48109-2140
and
J.-H. Chen‡
National Cheng-Kung University, Tainan 701, Taiwan, Republic of China

The properties of turbulence generated by uniform fluxes of polydisperse spherical particles moving through uniform flowing air are studied experimentally, emphasizing the properties of the turbulent interwake region surrounding the individual particle-wake disturbances. Mean and fluctuating velocities, as well as probability density functions, energy spectra and integral and Taylor length scales of velocity fluctuations, were measured within a counterflow particle/air wind tunnel using particle-wake discriminating laser velocimetry. Test conditions involved various binary mixtures of spherical glass particles having nominal diameters of 0.55, 1.1, and 2.2 mm and particle Reynolds numbers of 106, 373, and 990. When combined with earlier measurements limited to monodisperse spherical glass particles, the test conditions included mean particle spacings of 13–208 mm, particle volume fractions less than 0.003%, direct rates of dissipation of turbulence kinetic energy by particles less than 4%, and turbulence generation rates sufficient to yield streamwise and cross-stream gas velocity fluctuations, normalized by the streamwise mean velocity of the particles relative to the gas, in the range 0.2–1.5%. The turbulent interwake region for these conditions has properties that correspond to the final-decay period of grid-generated turbulence, including homogeneous and nearly isotropic turbulence having probability density functions that were well approximated by Gaussian functions with turbulence Reynolds numbers of 0.4–3.5. Mixing rules were developed, which successfully extended earlier results for the interwake turbulence properties of monodisperse particle phases to polydisperse particle phases, based on dissipation weighting of the properties of each particle size group. The flow in the final-decay period consisted of vortical regions that filled the turbulent interwake region but were sparse, which resulted in several unusual features of this region compared to conventional isotropic turbulence, as follows: enhanced rates of dissipation of turbulence kinetic energy, unusually large ratios of integral/Taylor length scales for conditions involving small turbulence Reynolds numbers, and decreasing ratios of integral/Taylor length scales with increasing turbulence Reynolds numbers, which is just opposite to the behavior of conventional grid-generated turbulence at large turbulence Reynolds numbers. The large range of scales where effects of viscosity were small in the final-decay region also yielded a Kolmogorov-like $-\frac{5}{3}$ power inertial decay region of one-dimensional energy spectra on dimensional grounds, similar to the inertial decay region of conventional turbulence at large turbulence Reynolds numbers.

Nomenclature

A	=	dimensionless integral length scale; Eq. (18)
C_d	=	particle drag coefficient
D	=	dissipation factor; Eqs. (9) and (11)
D_i	=	dissipation factor for particle size group i, Eq. (10)
d_p	=	particle diameter
$E(k)$	=	three-dimensional energy spectrum function
$E_u(k_u)$	=	streamwise one-dimensional energy spectrum function
$g(k\ell_K)$	=	dimensionless energy spectrum function; Eq. (14)
K	=	kurtosis of a probability density function
k	=	wave number
k_u	=	wave number in streamwise direction, $2\pi/s_u$
L_u	=	streamwise integral length scale
ℓ_K	=	Kolmogorov length scale, $(\nu^3/\varepsilon)^{1/4}$
ℓ_p	=	mean particle spacing; Eq. (1)
M	=	mesh size of a grid
N	=	number of particle size groups
n	=	power in isotropic turbulence decay law; Eq. (6)
n''	=	particle number flux
Re	=	particle Reynolds number, $d_p U_p/\nu$
Re_λ	=	turbulence Reynolds number, $\lambda\bar{u}'/\nu$
S	=	skewness of a probability density function
s_u	=	wavelength in streamwise direction
U_p	=	mean streamwise relative velocity of a particle
u	=	streamwise gas velocity
u_K	=	Kolmogorov velocity scale, $(\varepsilon\nu)^{1/4}$
v	=	cross-stream gas velocity
x	=	streamwise distance
x_o	=	streamwise virtual origin location
β	=	empirical factor; Eqs. (6–8)
ε	=	rate of dissipation of turbulence kinetic energy
ζ	=	generic variable
θ	=	particle-wake momentum diameter, $(C_d d_p^2/8)^{1/2}$
λ	=	Taylor dissipation length scale; Eq. (5)
ν	=	molecular kinematic viscosity of air
τ_K	=	Kolmogorov timescale, $(\nu/\varepsilon)^{1/2}$

Subscripts

b	=	particle size group of a binary mixture having the larger diameter
i	=	particle group i

Received 23 August 2002; presented as Paper 2003-1164 at the AIAA 41st Aerospace Sciences Meeting, Reno, NV, 6–9 January 2003; revision received 14 March 2003; accepted for publication 21 March 2003.

*Graduate Student Research Assistant, Department of Aerospace Engineering.
†A. B. Modine Professor, Department of Aerospace Engineering, 3000 François-Xavier Bagnoud Building, 1320 Beal Avenue. Fellow AIAA.
‡Assistant Professor, Department of Naval Architecture and Marine Engineering.

s = particle size group of a binary mixture having the smaller diameter

Superscripts

$(\bar{\ })$ = mean value
$(\bar{\ })'$ = rms fluctuating value

Introduction

TURBULENCE generation is the main source of turbulence in the dense (near-injector) region of sprays as well as in some natural dispersed multiphase flows, for example, rainstorms and hailstorms. Early studies showed that turbulence generation caused by particles (drops) involved particle wakes embedded in a turbulent interwake region.[1,2] Subsequent studies showed that the particle wakes scaled similar to laminar wakes but exhibited fast mixing as a result of the presence of turbulence (and as a result were called "laminar-like turbulent wakes").[3–6] More recent studies of monodisperse particle flows[7,8] showed that the turbulent interwake region consisted of isotropic turbulence in the rarely observed final-decay period, defined by Batchelor and Townsend[9,10] more than 50 years ago. The properties of isotropic turbulence in the final-decay period will be discussed in more detail later and are also considered by Batchelor and Townsend[9,10] and references cited therein. The main features of isotropic turbulence in the final-decay period are as follows: turbulence in the final-decay period fills the flow but is sparse so that measurements at a given point in the fluid exhibit the presence of turbulence as intermittent turbulent spots; in addition, turbulence in the final-decay period decays much more rapidly than conventional fully developed turbulence in the initial-decay period. During recent studies of turbulence generation,[7,8] an analogy was developed between grid-generated isotropic turbulence and particle-generated isotropic turbulence, when both were in the final-decay period, that provided useful correlations for the properties of the turbulent interwake region for monodisperse particle flows. This analogy was expressed in terms of the rate of dissipation of mechanical energy of the particles, which is known from the drag properties and motion of the particles relative to the continuous phase. The objective of the present experimental investigation was to develop mixing rules to extend these ideas to dispersed particle flows involving polydisperse particle phases.

Present measurements were carried out in a vertical counterflow particle/air wind tunnel. Binary particle pairs involving various proportions of nearly monodisperse glass spheres were considered. The properties of the mixing rules that were developed, however, suggest that this information can be extended to flows involving more general variations of particle sizes in a straightforward manner. As a result, the dispersed phase is simply called a polydisperse particle phase in the following. Measurements of the interwake region were made using particle-wake discriminating laser velocimetry (LV) to find the moments and the probability density functions (PDFs) of streamwise and cross-stream velocities, the one-dimensional energy spectra of streamwise velocity fluctuations, and the characteristic micro- and macrolength scales (streamwise integral and Taylor dissipation length scales) of the interwake turbulence. These results were interpreted and correlated similar to Ref. 7 by developing analogies between the turbulent interwake region of turbulence generation processes caused by particles and homogeneous grid-generated turbulence, for example, the studies of grid-generated turbulence of Refs. 9–22 and references cited therein.

Experimental Methods

Test Apparatus

The apparatus consisted of a vertical counterflow wind tunnel with upflowing air moving toward the suction side of the blower and with freely falling spherical glass particles introduced at the top of the wind tunnel (see Chen[23] for a complete description of the apparatus). Various binary particle mixtures were considered, with each particle size group in the mixture being nearly monodisperse, using individual particle feeders for each particle size of the mixture. The air flowpath consisted of a rounded inlet, a flow straightener, and a 16:1 contraction ratio to a windowed test section having a 305×305 mm cross section. The particle flowpath consisted of a variable-speed particle feeder for each particle size, a screen array particle dispersion section, a honeycomb particle flow straightener, and a particle acceleration section to yield particles having nearly terminal streamwise velocities in the test section. The particles were collected in a flexible plastic funnel below the air inlet. The particles were not damaged during passage through the apparatus; therefore, they were washed with detergent, dried, and sieved to retrieve the original particle sizes so that they could be reused.

Instrumentation

Techniques used to measure particle number fluxes, gas velocities, and particle velocities will only be discussed briefly because they have been fully described earlier.[6–8] Particle number fluxes were measured by collecting particles for timed intervals in a thin-walled cylinder closed at the bottom. The experimental uncertainties (95% confidence) of these measurements were less than 10%.

Gas velocities were measured using a single channel LV, rotating the optical plane in order to measure streamwise and cross-stream velocities. Velocities were found from the low-pass filtered analog output of the LV burst counter signal processor, using frequency shifting and a constant sampling rate of the burst counter output to eliminate effects of directional bias, directional ambiguity, and velocity bias. Heavy LV seeding levels were used so that effects of LV step noise were deferred to scales roughly an order of magnitude larger than the Kolmogorov scales. Tests with various seeding levels, however, showed that the LV seeding had essentially no effect on continuous phase turbulence properties. A particle detector was installed just above the LV sampling location, as discussed by Chen and Faeth.[7] Given the output of this detector and the known properties of laminarlike turbulent wakes, portions of the velocity signals that were in the particle-wake region were eliminated, providing conditional records of the velocity properties of the turbulent interwake region alone. For present test conditions LV signal dropout periods caused by particle-wake disturbances were in the range 7–31%.

LV velocity records, having drop-out periods that resulted when disturbances caused by particle wakes were removed, were analyzed directly by correcting the sampling time for most velocity statistics, for example, moments and PDF properties. In contrast, obtaining correct temporal power spectra in the presence of drop-out periods requires special treatment as discussed by Buchhave[24] and Buchhave et al.[25] (See Ref. 23 for the present application of these methods.) Upflow mean velocities in the wind tunnel were selected to provide absolute turbulence intensities smaller than 15% so that LV measuring conditions were excellent.[26] As a result, Taylor's hypothesis could be used to convert the measured temporal power spectra and scales to spatial one-dimensional energy spectra and scales of streamwise velocities. Sampling periods were adjusted to provide experimental uncertainties (95% confidence) less than 5% for mean streamwise velocities, less than 10% for streamwise and cross-stream rms velocity fluctuations, less than 10% for PDFs within one standard deviation of the most probable velocity and less than 20% for temporal power spectra at frequencies smaller than the reciprocal of the temporal integral scale with reduced uncertainties elsewhere.

Particle velocities were measured using the same LV arrangement. One difference, however, was that the LV optics were changed to increase the measuring volume diameter by a factor of roughly 30 to 1.5 mm and the measuring volume length by roughly a factor of 20 to 10 mm so that the larger measuring volume provided a reasonable sampling rate for particle velocities. The gas was not seeded during the particle velocity measurements, and the large-amplitude signals from the glass particles were easily separated from background signals caused by dust particles in the air. Experimental uncertainties (95% confidence) of streamwise mean particle velocities were less than 5%.

Test Conditions

Particle properties are summarized in Table 1. Each particle size group was nearly monodisperse and spherical and had nominal diameters of 0.5, 1.1, and 2.2 mm and corresponding Reynolds

Table 1 Summary of particle properties[a]

Parameter	Nominal particle diameter, mm[b] 0.5(0.05)	1.1(0.1)	2.2(0.1)
U_p, mm/s	3,370(28)	5,530(340)	7,000(200)
Re	106(9)	373(23)	990(28)
C_d	1.22	0.79	0.54
$d\ell nU_p/dx$, %/m	2	11	14
θ, mm	0.183	0.299	0.519

[a]Round glass beads (density of 2500 kg/m^3) falling in upflowing air at normal temperature and pressure (air density of 1.16 kg/m^3 and kinematic viscosity of 15.9 mm^2/s) having a mean upflow velocity of 1.1 m/s.
[b]Standard deviations of properties given in parentheses.

Table 2 Test conditions for binary particle phases[a]

Parameter	Particle diameters in binary particle mixtures, mm 0.5 and 1.1	0.5 and 2.2	1.1 and 2.2
n''_s, kpart/m^{2}s	95–556	95–556	4–32
n''_b, kpart/m^{2}s	4–27	0.8–6.4	0.8–6.4
ℓ_p, mm	16–29	16–26	49–99
ε, m^2/s^3	0.17–1.10	0.22–1.10	0.085–0.69
ℓ_K, mm	0.2–0.4	0.2–0.4	0.3–0.5
τ_K, ms	10–30	2–4	5–14
u_K, mm/s	41–64	43–64	34–57
$\bar{u}'/U_p$, %	0.6–1.4	0.6–1.4	0.2–0.6
λ, mm	0.6–0.8	0.7–0.8	0.5–0.7
Re_λ	0.9–2.3	0.9–2.4	0.4–1.6
L_u, mm	10–109	14–134	50–148

[a]Binary mixtures of round glass beads in upflowing air at normal temperature and pressure with particle and gas properties given in Table 1. Measurements from the present investigation.

Table 3 Test conditions for monodisperse particle phases[a]

Parameter	Nominal particle diameter, mm 0.5	1.1	2.2
n'', kpart/m^{2}s	71–950	4–56	0.5–10
ℓ_p, mm	13–32	41–97	77–208
ε, m^2/s^3	0.088–1.17	0.041–0.54	0.012–2.3
ℓ_K, mm	0.2–0.5	0.3–0.6	0.4–0.7
τ_K, ms	4–14	5–16	8–37
u_K, mm/s	34–60	31–54	21–44
$\bar{u}'/U_p$, %	0.5–1.5	0.2–0.6	0.2–0.6
λ, mm	0.7–0.9	0.6–0.8	1.2–1.8
Re_λ	0.7–2.5	0.4–1.5	1.4–3.5
L_u, mm	11–35	42–178	23–156

[a]Monodisperse round glass beads in upflowing air at normal temperature and pressure with particle and air properties given in Table 1. Measurements from Chen and Faeth.[7]

numbers of 106, 373, and 990. The particle Reynolds numbers are representative of the intermediate Reynolds number conditions typical of drops providing significant degrees of turbulence generation in sprays.[3] Terminal velocities and drag coefficients were measured, yielding values that agreed with the standard drag curve for spheres, from Putnam,[27] within 15%. The particles approached but did not reach terminal velocity conditions during the present measurements, for example, rates of particle acceleration at the measuring location were 2, 11, and 14% of the mean particle velocities per meter for the three particle size groups. Finally, cross-stream mean particle velocities and streamwise and cross-stream particle velocity fluctuations (excluding streamwise velocity variations associated with varying particle diameters) were small because of the large inertia and poor particle response to air motion of the present particles.

Test conditions for the various binary particle phases that were considered are summarized in Table 2. Results from Chen and Faeth[7] for monodisperse particle phases were combined with the present results for binary particle phases, after developing appropriate mixing rules for the binary particle phases; therefore, the test conditions for the various monodisperse particle phases considered by Chen and Faeth[7] are summarized in Table 3 for reference purposes.

Assuming that the particles are monodisperse and are falling randomly, the mean particle spacing can be found from[6]

$$\ell_p = [(U_p - \bar{u})/n'']^{\frac{1}{3}} \tag{1}$$

This expression was modified to treat the present binary particle phases using dissipation-weighted averaging to find an average U_p that will be described subsequently. For the combined monodisperse and binary particle phase test conditions considered here, mean particle spacings were in the range 13–208 mm with corresponding particle volume fractions less than 0.003%.

The direct dissipation of turbulence kinetic energy (dissipation) by particles was less than 4% for all test conditions (see Chen[23] for a discussion of this estimate). In addition, dissipation within the wake disturbances was also small, less than 12% of the total dissipation, as discussed by Chen and Faeth[7] for all test conditions. As a result, the rate of dissipation within the turbulent interwake region can be found from the rate of turbulence generation by the particles, where ε_i is the rate of dissipation of particle group i, as follows:

$$\varepsilon_i = \pi \dot{n}''_i \left(d_p^2 C_d U_p^2 / 8\right)_i \tag{2}$$

and the total dissipation given N particle size groups is found by summing the contributions of each particle size group, as follows:

$$\varepsilon = \sum_{i=1}^{N} \varepsilon_i \tag{3}$$

Given ε, the Kolmogorov length, time, and velocity scales for the turbulent interwake region can be computed from their definitions, as follows[28]:

$$\ell_K = (\nu^3/\varepsilon)^{\frac{1}{4}}, \qquad \tau_K = (\nu/\varepsilon)^{\frac{1}{2}}, \qquad u_K = (\nu\varepsilon)^{\frac{1}{4}} \tag{4}$$

Thus, given the ranges of ε, the ranges of these scales can be found from Eqs. (4) as summarized in Tables 2 and 3 for binary and monodisperse particle phases, respectively. For these same dissipation rates the relative turbulence intensities caused by turbulence generation ($\bar{u}'/U_p$ and $\bar{v}'/U_p$) were in the range 0.2–1.5%, based on the dissipation weighted value of U_p that will be discussed later. Similar to the earlier measurements for monodisperse particle phases,[7] the present measurements also indicate that interwake turbulence is similar to homogeneous isotropic turbulence so that the Taylor dissipation length scale can be estimated as follows:

$$\lambda = (15\nu\bar{u}'^2/\varepsilon)^{\frac{1}{2}} \tag{5}$$

The resulting values of λ for all test conditions are comparable but somewhat larger than the Kolmogorov scales (e.g., $\lambda/\ell_K = 1.3$–3.5). The corresponding range of turbulence Reynolds numbers for all test conditions, $Re_\lambda = \lambda\bar{u}'/\nu$, is 0.4–3.5, which is relatively small, helping to explain why the Taylor and Kolmogorov length scales are nearly the same. Streamwise integral length scales were obtained from the energy spectra as discussed later, yielding values of 10–178 mm, which are comparable to the mean particle spacings, for all test conditions.

Finally, evaluation of the apparatus for binary particle phases yielded results very similar to earlier evaluation of the apparatus for monodisperse particle phases.[6,23] In particular, particle number fluxes and phase velocities varied less than experimental uncertainties over the central 205 × 205-mm cross section of the flow, extending 200 mm in the streamwise direction, which surrounded the location where measurements were made. The measurements also showed that flow properties varied less than experimental uncertainties as a function of time. Thus, the present flows were properly homogeneous and stationary, with the turbulence within the turbulence interwake region produced by turbulence generation, as desired.

Results and Discussion

Relative Turbulence Intensities

Batchelor and Townsend[9,10] defined three regions of turbulence downstream of a turbulence-producing grid, as follows: 1) a developing period near the grid where wakes from grid elements are merging and the flow is neither homogeneous nor isotropic; 2) an initial-decay period, where the turbulent flow is homogeneous and locally isotropic; and 3) a final-decay period, where effects of fluid inertia forces are negligible so that the governing Navier–Stokes equations of the flow become linear, where regions containing vorticity become sparse (giving the appearance of isolated turbulent spots based on single-point measurements) and where the turbulence decays more rapidly than in the initial-decay region. Based on the earlier observations of flows caused by turbulence generation caused by monodisperse particles,[7] it appears that the final-decay period is associated with the turbulent interwake region of these flows. Supporting this idea is the fact that $Re_\lambda \leq 3.5$ for the conditions of both past observations of the interwake region for monodisperse particle phases and for present observations of the interwake region for polydisperse particle phases, whereas Batchelor and Townsend[9,10] suggest a value of $Re_\lambda < 5$ as the condition for the presence of the final-decay period of grid-generated turbulence.

The analogy between grid-generated turbulence and the turbulent interwake region developed in Ref. 7 was based on the following expression for grid-generated turbulence from Batchelor and Townsend[9,10]:

$$(\bar{u}' \quad \text{or} \quad \bar{v}')/\bar{u} = \beta[C_d M/(x - x_o)]^n \tag{6}$$

where $(x - x_o)$ is the distance of the point of observation from the virtual origin of the grid. In addition, they find, based on both analysis and measurements that $n = \frac{1}{2}$ and $\frac{5}{4}$ for the initial- and final-decay periods, respectively. The various parameters of Eq. (6) for grid-generated turbulence were then related to the parameters of the turbulent interwake region, as follows[7]: the length corresponding to the product of the mesh size and the drag coefficient of grid-generated turbulence were taken to be the particle-wake momentum diameter θ, which similarly involves the product of the size of an element resistive to flow motion and its drag coefficient; the distance from the grid for grid-generated turbulence was taken to be on the order of the mean particle spacing for the homogeneous turbulent interwake region assuming that this represents the open or undisturbed region where the turbulent interwake region can develop; and the mean velocity of the continuous phase relative to the grid for grid-generated turbulence was taken to be the mean velocity of the particles relative to the velocity of the continuous phase for the turbulent interwake region. Given these analogies, the expression corresponding to Eq. (6) for the turbulent interwake region becomes

$$(\bar{u}' \quad \text{or} \quad \bar{v}')/U_p = \beta(\theta/\ell_p)^n \tag{7}$$

where β may not necessarily be the same for $\bar{u}'$ or $\bar{v}'$. Then noting that $\theta = (C_d d_p^2/8)^{1/2}$, finding ℓ_p from Eq. (1) and eliminating n'' from the resulting equation using Eqs. (2) and (3) (appropriately averaged for polydisperse particle phases as will be discussed subsequently), yields the following correlation for the relative turbulence intensities of the turbulent interwake region:

$$(\bar{u}' \quad \text{or} \quad \bar{v}')/U_p = \beta D^{n/3} \tag{8}$$

where D is a dimensionless dissipation factor defined as follows for monodisperse particle phases[7]:

$$D = (\theta/\ell_p)^3 = \frac{\varepsilon d_p (C_d/8)^{\frac{1}{2}}}{\left[\pi U_p^2 (U_p - \bar{u})\right]} \tag{9}$$

The modification of the expression for D needed to treat polydisperse particle phases will be discussed next.

Dissipation-weighted averaging was used to treat polydisperse particle phases based on the particle dissipation factor for particle size i, as follows:

$$D_i = \frac{\varepsilon_i d_{\text{pi}} (C_{\text{di}}/8)^{\frac{1}{2}}}{\left[\pi U_{\text{pi}}^2 (U_{\text{pi}} - \bar{u})\right]} \tag{10}$$

The flow dissipation factor was then taken to be the sum

$$D = \sum_{i=1}^{N} D_i \tag{11}$$

Finally, to complete the mixing rules needed to treat polydisperse particle phases dissipation-weighted averaging was used to find the effective relative particle velocity:

$$U_p = \sum_{i=1}^{N} \left(\frac{D_i}{D}\right) U_{\text{pi}} \tag{12}$$

The idea behind the mixing rules embodied by Eqs. (10–12) for polydisperse particle phases was to emphasize the fact that turbulence generation is created by the dissipation of the turbulence kinetic energy of the particle phase. This approach also avoids overweighting the importance of potentially large numbers of small particles on flow properties, for example, seeding particles having negligible slip that really would contribute very little to the properties of the interwake turbulent region caused by turbulence generation as a result of their small relative motion with respect to the continuous phase, and thus their small rates of dissipation of the kinetic energy of the particle phase.

Present measurements of streamwise and cross-stream relative turbulence intensities $\bar{u}'/U_p$ and $\bar{v}'/U_p$ within the turbulent interwake region of all of the binary particle mixtures considered during the present experiments are plotted in Fig. 1 according to Eq. (8), in conjunction with the mixing rules for polydisperse particles of Eqs. (10–12). Earlier results from Ref. 7 for monodisperse particles are also shown on the figure, plotted in the same manner [noting that the mixing rules of Eqs. (11) and (12) properly retrieve the

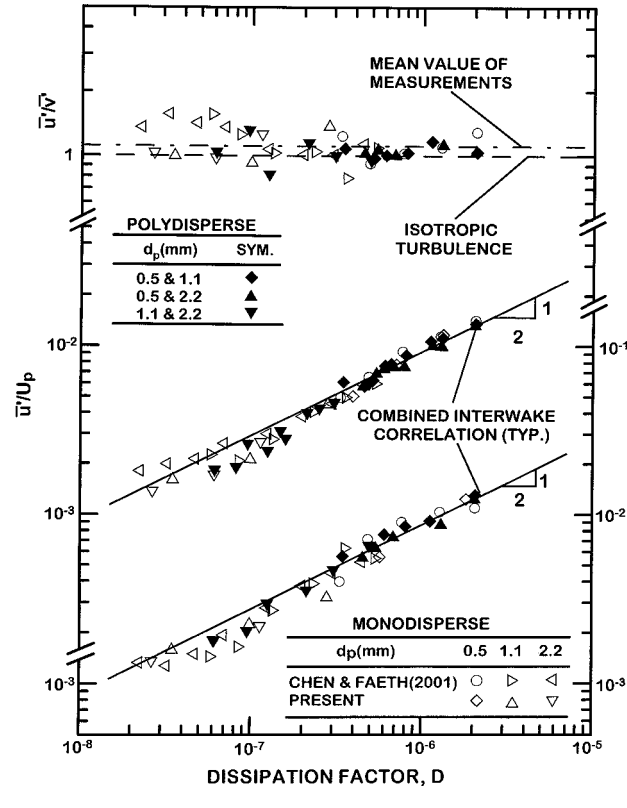

Fig. 1 Streamwise and cross-stream relative turbulence intensities $\bar{u}'/U_p$ and $\bar{v}'/U_p$ and anisotropy factors $\bar{u}'/\bar{v}'$ as a function of the dissipation factor for various monodisperse and polydisperse particle phases. Particle-generated turbulence measurements of Chen and Faeth[7] and the present investigation.

original formulation for monodisperse particles]. The correlation of the results for both monodisperse and polydisperse particle phases is seen to be remarkably good, for the roughly two orders of magnitude range of D that spans the data. Best-fit correlations of the data yielded powers of D in the correlations Eqs. (8) of $\frac{1}{2}$ within experimental uncertainties (95% confidence), as follows:

$$\bar{u}'/U_p = 9.3D^{\frac{1}{2}}, \qquad \bar{v}'/U_p = 8.7D^{\frac{1}{2}} \tag{13}$$

with the standard deviations of both coefficients of Eqs. (13) of 1.2 and with the correlation coefficients of these fits of 0.98 and 0.96, respectively, which is excellent. The powers of D in Eq. (13) suggest that $n = \frac{3}{2}$ from Eq. (8), which is reasonably close to the value of $n = \frac{5}{4}$ for the final-decay period suggested by Batchelor and Townsend.[9,10] (The results of Fig. 1 also agree with the estimate that the present turbulent interwake regions should be in the final-decay period because $Re_\lambda < 3.5$ for these flows.)

The ratio of the coefficients of Eqs. (13) yields a mean value of the anisotropy factor $\bar{u}'/\bar{v}'$ over the present test range of 1.07. The difference between this value of the anisotropy factor and unity is not statistically significant for the present measurements; therefore, present findings suggest that the turbulent interwake region is isotropic within the limitations of the present measurements of these properties. This matter is also considered in Fig. 1, where individual values of $\bar{u}'/\bar{v}'$ from Chen and Faeth[7] and from the present investigation are plotted. These results yield values of the anisotropy ratio [with experimental uncertainties (95% confidence) in parentheses] as follows: 1.17 (0.10) for the results of Chen and Faeth,[7] 1.06 (0.05) for the present results, and 1.11 (0.05) for the combined results from both investigations. In view of these measurements, and the potential for a slight upward bias of $\bar{u}'$, and thus $\bar{u}'/\bar{v}'$, because of incompletely removed wake disturbances (to be discussed subsequently), it cannot be concluded that the present results exhibited significant degrees of anisotropy. On the other hand, others have found evidence for anisotropic behavior for isotropic turbulence having small Reynolds numbers, for example, Bennett and Corrsin[29] observe values of the anisotropy ratio of 1.09–1.22 for isotropic turbulence having relatively small Reynolds numbers ($Re_\lambda = 36$–72). Thus, small levels of anisotropy cannot be discounted for present measurements of the turbulent interwake region pending additional study.

PDFs

Typical measured PDFs of streamwise and cross-stream velocities in the turbulent interwake region for various polydisperse particle phases are illustrated in Figs. 2 and 3. Best Gaussian fits of the measurements are also shown on the plots. The PDFs are plotted using logarithmic coordinates in order to highlight potential effects of wake disturbances and the performance of the fits at the extremities of the distributions where the PDFs become small.

The PDFs for polydisperse particle phases illustrated in Figs. 2 and 3 are essentially identical to the earlier results illustrated in Ref. 7 for monodisperse particle phases. Thus, there are no obvious bimodal properties of the velocity fluctuations caused by the bimodal nature of the dispersed phase as well as the bimodal properties of the dispersed-phase wakes. The cross-stream PDFs illustrated in Fig. 3 are symmetric and are in generally good agreement with the Gaussian fits except for slight upward biases near both ends of the distributions. These biases are thought to be caused by sampling limitations because the values of the PDFs are very small in this region, ca. 10^{-3}, which requires a larger number of samples to properly resolve than was feasible for the present experiments.

The PDFs of streamwise velocity fluctuations illustrated in Fig. 2 are clearly asymmetric with an upward bias of the distributions roughly near -2.5 standard deviations from the mean. Because a similar upward bias is absent from the cross-stream PDFs, which have no disturbances from mean velocities in the randomly arriving particle wakes,[4] this bias is probably caused by small disturbances from mean velocities in the randomly arriving particle wakes that were not completely eliminated by the present wake discrimination system. See Chen and Faeth[7,8] for additional considerations of PDFs for the turbulent interwake region and the effect of particle wake disturbances on these properties.

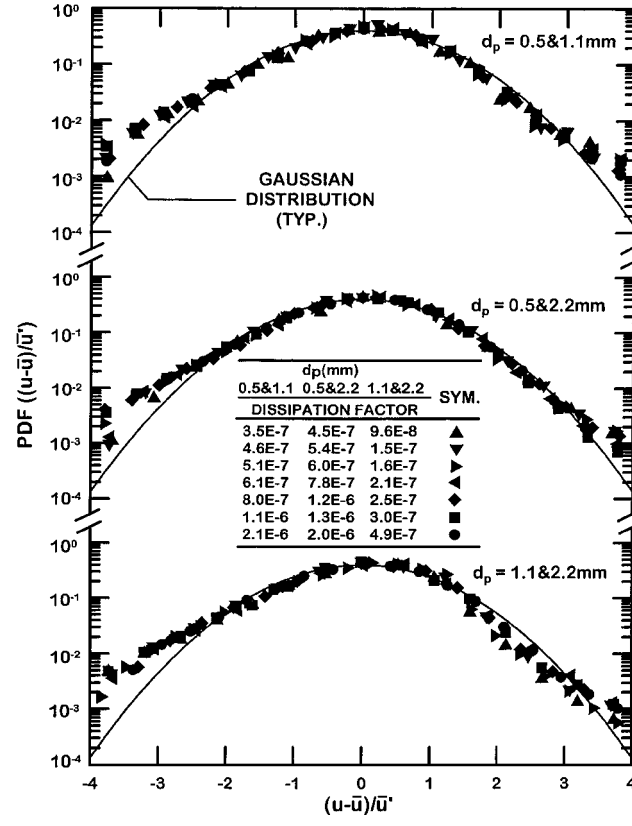

Fig. 2 Typical PDFs of streamwise velocity fluctuations for various polydisperse particle phases and dissipation factors from the present investigation.

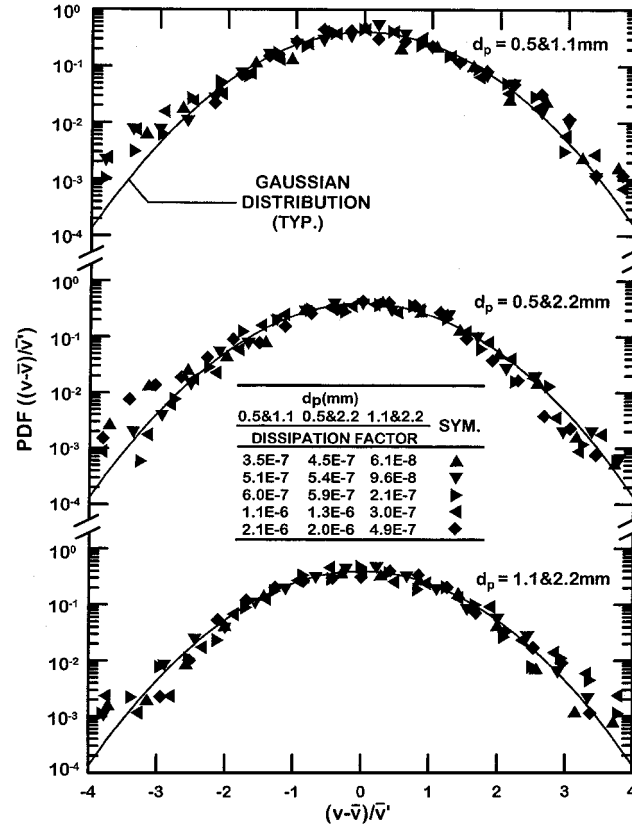

Fig. 3 Typical PDFs of cross-stream velocity fluctuations for various polydisperse particle phases and dissipation factors from the present investigation.

The rest of the properties of the PDFs for polydisperse particle phases were also the same as for monodisperse particle phases, as follows (giving standard deviations in parentheses): $S(u)$ and $S(v)$ are $-0.6(0.2)$ and $0.0(0.3)$, respectively; and values of $K(u)$ and $K(v)$ are 5(1) and 4(1), respectively. The departures of $S(u)$ and $S(v)$ from the Gaussian value of $S=0$ are not statistically significant; the departures of $K(u)$ and $K(v)$ from the Gaussian value of $K=3$ also border on statistical significance particularly in view of the larger experimental uncertainties of this higher-order moment caused by sampling limitations. These findings were similar to results for $S(u)$, $S(v)$, $K(u)$, and $K(v)$ from the earlier tests for monodisperse particle phases,[7] supporting the absence of bimodal behavior of the interwake region caused by turbulence generation by bimodal particle phases.

Taking all of the information about the PDFs of u and v together, both from Chen and Faeth[7] and the present study, it is concluded that they are adequately described for practical purposes by Gaussian functions, as anticipated for turbulence in the final-decay period.[9,10] In this respect the present flows in the final-decay period behave similar to other isotropic turbulent flows that have been studied.[26,28]

One-Dimensional Energy Spectra

The normalized one-dimensional energy spectra of streamwise velocity fluctuations of interwake turbulence for various binary pairs of dispersed-phase particles are illustrated in Fig. 4. The corresponding integral length scales were found by noting that the normalized amplitude of the one-dimensional streamwise energy spectra $2\pi E_u(k_u)/(\bar{u}'^2 L_u)$ approaches the value of four when the normalized wave number on these plots $k_u L_u/(2\pi)$ becomes small as discussed by Hinze.[26] Correlations of the one-dimensional streamwise energy spectra for approximate isotropic turbulence that satisfy the small wave-number limit of four are also shown on the plot for comparison with the measurements; these approximate spectra represent a simplification of isotropic turbulence, where correlations of velocity fluctuations are assumed to satisfy an exponential function.[26] The exponential function spectra yield a rate of decay of the spectra in the inertial region of -2, which is marked on the plot. In addition, as will be discussed subsequently, the present interwake turbulence in the final-decay period has an extensive inertial-like decay region so that its three-dimensional energy spectra should exhibit a corresponding $-\frac{5}{3}$ Kolmogorov-like decay region at large wave numbers. Furthermore, Hinze[26] has established that if the three-dimensional energy spectrum $E(k)$ can be represented by a power law function of the wave number for a wave-number range $k_u \le k < \infty$, then the one-dimensional energy spectrum $E_u(k_u)$ will obey the same power law for this wave-number range, and vice versa. Motivated by these findings, the measured one-dimensional energy spectra for the present interwake turbulence in Fig. 4 have been fitted to a $-\frac{5}{3}$ Kolmogorov-like decay law for values of $k_u L_u/(2\pi) > 0.6$. This region does not extend to smaller wave numbers as a result of disturbances of the spectra caused by mean velocities in randomly arriving wake disturbances, creating a slight bulge in the spectra near a dimensionless wave number of 0.1 (Refs. 6 and 7). Finally, the range of $k_u L_u/(2\pi)$ associated with wave numbers characteristic of Kolmogorov scales are also indicated on the plot in order to provide an indication of the full range of scales associated with present test conditions within the turbulent interwake region, not just the range that could be considered as a result of the limitations caused by step noise, as well as the conditions where effects of viscosity become important in these flows.

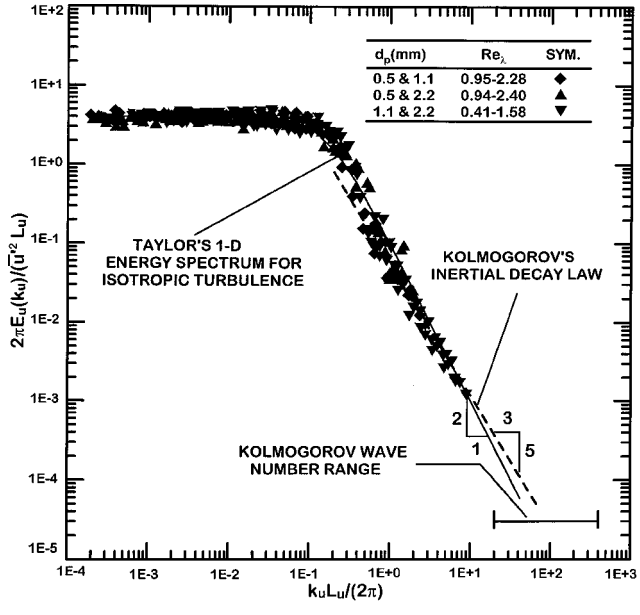

Fig. 4 Typical one-dimensional energy spectra of streamwise velocity fluctuations for various polydisperse particle phases and turbulence Reynolds numbers from the present investigation.

The one-dimensional energy spectra illustrated for polydisperse particle phases in Fig. 4, along with previous results for monodisperse dispersed phases illustrated in Ref. 7, are independent of particle properties and total dissipation rates and agree reasonably well with the isotropic turbulence approximation of Hinze[26] at relatively small wave numbers [$k_u L_u/(2\pi) < 0.6$]. These spectra also have a Kolmogorov-like $-\frac{5}{3}$ energy decay range in the inertial region at large wave numbers [$k_u L_u(2\pi) > 0.6$]. In fact, within the wave-number range just mentioned, the fitted slope of the present one-dimensional energy spectra is -1.68 with an uncertainty (95% confidence) of 0.18 and a correlation coefficient of the fit of 0.87, which agrees with the -1.67 Kolmogorov slope within statistical significance. Finally, as noted earlier, the measured spectra are truncated at significantly smaller wave numbers than those associated with Kolmogorov scales in order to avoid step noise caused by sampling limitations. The full range of scales between the integral and Kolmogorov scales is surprisingly large; however, roughly 1000:1, even though the turbulence Reynolds numbers for these conditions were all smaller than 3.5. This behavior highlights some of the unusual properties of turbulence in the final-decay period compared to conventional turbulence. Subsequent consideration of the integral and Taylor-dissipation length scales of the turbulent interwake regions associated with turbulence generation, however, will show that these large ranges of scales represent reasonable behavior for turbulence in the final-decay period.

It is widely recognized that the one-dimensional energy spectra $E_u(k_u)$ of conventional isotropic turbulence having large turbulence Reynolds numbers should exhibit an extended $-\frac{5}{3}$ Kolmogorov decay law for the inertial range of the turbulence, which involves the wave-number range $k_u L_u \sim 1$ to $k_u \lambda \sim 1$. An interesting question raised by present results is why should turbulence in the final-decay period having small turbulence Reynolds numbers, as illustrated in Fig. 4, also exhibit a $-\frac{5}{3}$ Kolmogorov-like inertial decay region for the extended wave-number range $k_u L_u \sim 1$ to $k_u \lambda \approx k_u \ell_K \sim 1$ illustrated in Fig. 4. This behavior is discussed in the following based on consideration of the three-dimensional energy spectra, which is typical of most derivations of the Kolmogorov decay law; the findings of Hinze[26] will be exploited subsequently to relate results for three-dimensional energy spectra to the one-dimensional energy spectra that were measured during the present investigation and are plotted in Fig. 4. Similar to conventional turbulence at large turbulence Reynolds numbers, the Kolmogorov-like law follows from dimensional considerations alone because there is a large range of scales of turbulence in the final-decay period, with effects of viscosity confined to the high wave-number range associated with the Taylor-dissipation length scales of the flow (which are very nearly equal to the Kolmogorov length scales for present test conditions). In particular, noting that $E_u(k)$ has dimensions $m^3 s^{-2}$, whereas k has dimensions m^{-1}, the dimensionless energy spectra must have a form normalized by the Kolmogorov length scales and timescales, as follows:

$$\frac{E(k)}{\left(\ell_K^3 \tau_K^{-2}\right)} = g(k\ell_K) \tag{14}$$

Introducing the definitions of the Kolmogorov scales ℓ_K and τ_K from Eqs. (4), Eq. (14) becomes

$$E(k) = \nu^{\frac{5}{4}}\varepsilon^{\frac{1}{4}} g\left(k\nu^{\frac{3}{4}}\varepsilon^{-\frac{1}{4}}\right) \tag{15}$$

Finally, in order for $E(k)$ to be in the inertial range, where it is independent of ν, it is required that $g(\zeta) \sim \zeta^{-5/3}$, which implies

$$E(k) \sim \varepsilon^{\frac{2}{3}} k^{-\frac{5}{3}} \tag{16}$$

Finally, from the Hinze[26] relationship, given Eq. (16), the following must be true within the same wave-number range:

$$E_u(k_u) \sim k_u^{-\frac{5}{3}} \tag{17}$$

Thus, dimensional considerations alone require the presence of a $-\frac{5}{3}$ Kolmogorov-like inertial decay region for the one-dimensional energy spectra of interwake turbulence in the final-decay period at small turbulence Reynolds numbers, as seen in Fig. 4, similar to the familiar $-\frac{5}{3}$ Kolmogorov inertial decay region of conventional turbulence at large turbulence Reynolds numbers. This property of the final-decay period results from the large range of length scales present for turbulence in the final-decay period in spite of its small turbulence Reynolds numbers; this behavior is considered next.

Length Scales

The rate of dissipation of turbulence kinetic energy within conventional isotropic turbulence at large turbulence Reynolds numbers can be estimated from the values of the streamwise velocity fluctuations and integral length scales, using the following expression[26]:

$$A = \varepsilon L_u/(\bar{u}')^3 \tag{18}$$

where A is a constant on the order of unity for conventional isotropic turbulence at large turbulence Reynolds numbers. All properties on the right-hand side of Eq. (18) were measured during the studies of the turbulent interwake region of Ref. 7 and the present investigation, yielding values of A at various turbulence Reynolds numbers that will be considered next.

The available determinations of A for isotropic turbulence are plotted in Fig. 5 as a function of Re_λ. Results for isotropic turbulence in the final-decay period, at Re_λ in the range 0.4–3.5, are plotted on the figure based on measurements of Ref. 7 and the present investigation. Results for isotropic turbulence in the initial-decay period for $Re_\lambda = 20$–800 are also plotted in the figure, considering measurements,[11–15] direct numerical simulations (DNS),[16–19] and the DNS data fit of Sreenivasan.[20] The results in the initial-decay period for $Re_\lambda = 20$–800 involve fully developed isotropic turbulence that acts over the entire flowfield and yields values of A on the order of unity, as expected. The measurements in the final-decay period for the turbulent interwake region involving both monodisperse and binary particle phases at small Re_λ are in good agreement with each other but exhibit very enhanced rates of dissipation (at comparable magnitudes of streamwise integral length scales and rms velocity fluctuations) compared to conventional isotropic turbulence having large turbulence Reynolds numbers. This behavior is typical of behavior in the final-decay period, where the vorticity is sparse and the turbulence appears to consist of disconnected spots when single-point measurements are observed.[9,10,21,22] This behavior is also consistent with observations that interwake turbulence for present conditions was in the final-decay period, as discussed in connection with Fig. 1.

The measurements illustrated in Fig. 5 suggest that there are three regimes of isotropic turbulence based on the behavior of the dimensionless integral length scale, as follows: 1) the initial-decay period, 2) the final-decay period, and 3) a transition period separating the initial- and final-decay periods. The initial-decay period corresponds to classical isotropic turbulence at large turbulence Reynolds numbers with dimensionless integral length scale properties, as follows[20]:

$$0.3 \le A \le 2.0, \qquad \text{initial-decay period} \qquad (Re_\lambda > 100) \tag{19}$$

In this region the turbulence is fully developed and acts over the entire flow region. Sreenivasan[20] suggests that values of A vary

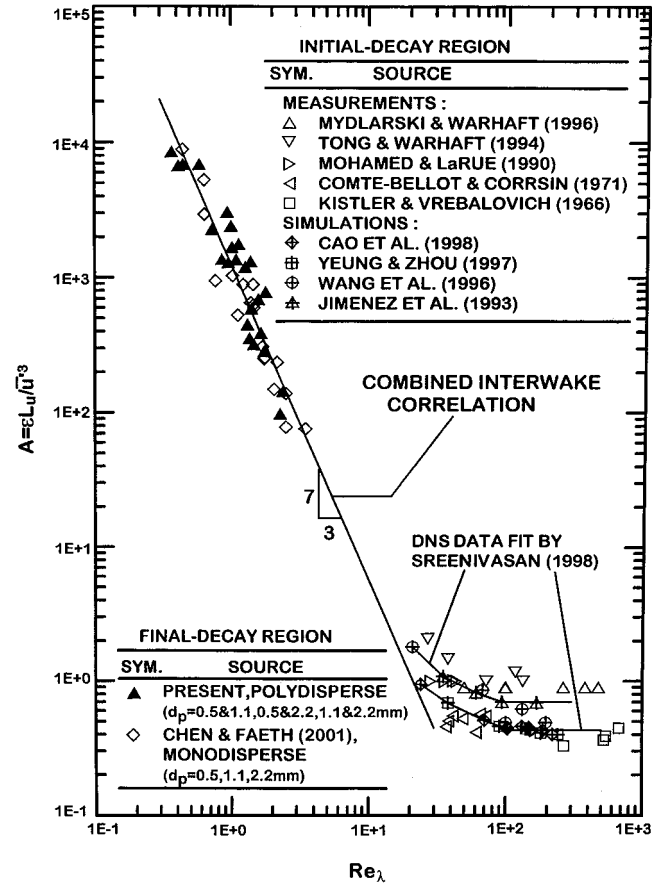

Fig. 5 Normalized integral length scales as a function of turbulence Reynolds number for both grid- and particle-generated turbulence. Grid-generated turbulence measurements of Refs. 11–15; particle-generated turbulence measurements of Ref. 7 and the present investigation; grid-generated turbulence predictions of Refs. 16–19; and grid-generated turbulence DNS fit of Ref. 20.

as a result of different initial conditions or grid geometries of the flows, but the values of A generally are subsequently independent of the turbulence Reynolds number. The measurements within the turbulent interwake region of Ref. 7 and during the present investigation correspond to the final-decay period of grid-generated isotropic turbulence, based on the discussion of Fig. 1, with dimensionless integral length-scale properties as follows, as illustrated in Fig. 5:

$$A = 1250 Re_\lambda^{-\frac{7}{3}}, \qquad \text{final-decay period} \qquad (Re_\lambda < 10) \tag{20}$$

where existing measurements of A in this region are limited to Re_λ of 0.4–3.5, the experimental uncertainty (95% confidence) of the power of Re_λ in Eq. (20) is 0.20, and the correlation coefficient of the fit is 0.90. Finally, there is a transition region between the initial- and final-decay periods where Ling and Huang[21] suggest

$$A = 33/Re_\lambda, \qquad \text{transition period} \qquad (10 \le Re_\lambda \le 100) \tag{21}$$

It also is of interest to consider the range of scales present in each of the three isotropic turbulence periods because this provides a more complete physical picture of the flows. This information can be developed by noting from Eqs. (5) and (17), and the definition of Re_λ, that the macroscale/microscale ratio L_u/λ is simply related to Re_λ as follows:

$$L_u/\lambda = ARe_\lambda/15 \tag{22}$$

in all of the periods of turbulence. As a result, the ratio of L_u/λ in the initial-decay period becomes, from Eqs. (19) and (22),

$$L_u/\lambda = ARe_\lambda/15, \qquad \text{initial-decay period} \qquad (Re_\lambda > 100) \tag{23}$$

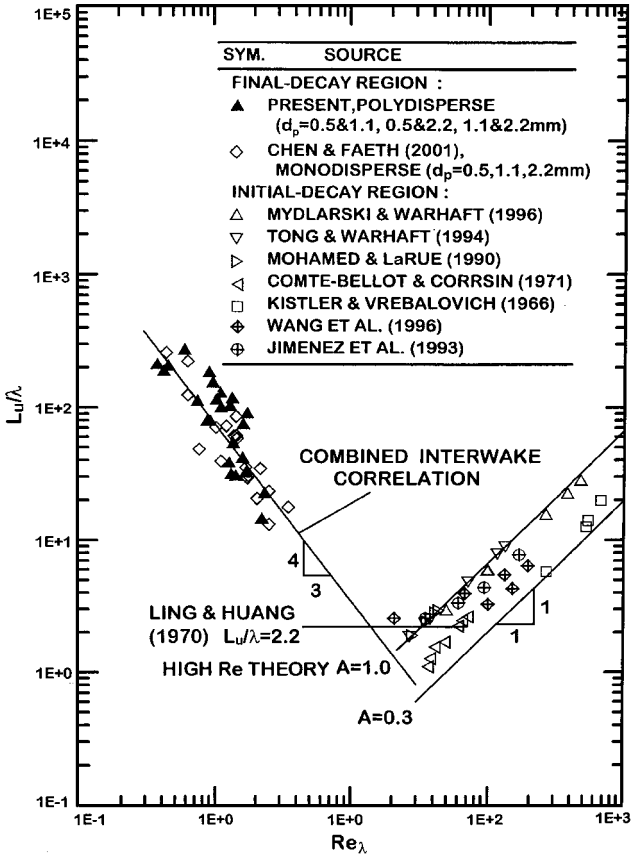

Fig. 6 Ratios of integral and Taylor length scales as a function of turbulence Reynolds number for both grid- and particle-generated turbulence. Grid-generated turbulence measurements of Refs. 11–15; particle-generated turbulence measurements of Ref. 7 and the present investigation; grid-generated turbulence predictions of Refs. 16 and 17; and grid-generated correlation of Ref. 21.

The length-scale ratio for the final-decay period becomes, from Eqs. (20) and (22),

$$L_u/\lambda = 83Re_\lambda^{-\frac{4}{3}}, \qquad \text{final-decay period} \qquad (Re_\lambda < 10) \quad (24)$$

Finally, the length-scale ratio for the transition period becomes, from Eqs. (21) and (22),

$$L_u/\lambda = 2.2, \qquad \text{transition period} \qquad (10 \le Re_\lambda \le 100) \quad (25)$$

The correlations of L_u/λ from Eqs. (23–25) are illustrated in Fig. 6 along with results from available measurements and DNS. Taken together, the various correlations provide reasonably good fits of available measurements and numerical predictions in the initial-decay, the final-decay, and the transition periods. This plot also suggests why there is a transition of the behavior of L_u/λ in going from the initial- to the final-decay periods of isotropic turbulence. For example, as Re_λ decreases in the initial-decay period L_u/λ progressively decreases and approaches unity as Re_λ approaches 100. Clearly, a macroscale, for example, L_u, cannot become smaller than a microscale, for example, λ, for a rational turbulent flow; therefore, it is not surprising that there is a transition to the final-decay period, for Re_λ in the range 10–100, which involves L_u/λ properly remaining larger than unity for additional reductions of Re_λ.

The increasing values of L_u/λ as Re_λ increases are well understood for conventional turbulence at large turbulence Reynolds numbers in the initial-decay period because the relatively large-scale features of the turbulence (on the scale of integral scales) are relatively independent of effects of viscosity, and thus Reynolds numbers, whereas the smallest scales of turbulence, represented by the Taylor dissipation and Kolmogorov length scales, become progressively smaller as Re_λ increases, which causes a corresponding increase of L_u/λ. The increase of L_u/λ with decreasing Re_λ in the final-decay period, however, occurs for very different reasons. In this case regions containing vorticity are sparse, but they still spread throughout the entire flow, yielding large integral length scales that progressively increase in size as the flow decays, in the presence of small dissipation length scales. Then, the continued spread of the flow, combined with relatively slow changes of dissipation length scales, implies progressively increasing values of L_u/λ as the flow decays (or as Re_λ decreases), as seen in Fig. 6. Thus, the main distinction between the two flows is that L_u/λ increases with increasing Re_λ for conventional turbulence in the initial-decay period because λ becomes smaller but increases with decreasing Re_λ for turbulence in the final-decay period because L_u becomes larger.

Conclusions

This investigation has considered the properties of turbulence generated by uniform fluxes of polydisperse particle phases moving through air at standard temperature and pressure, emphasizing the properties of the turbulent interwake region of this flow. Combined with the earlier study of Ref. 7, involving monodisperse particle phases, test conditions include particle phases consisting of monodisperse and binary mixtures of nearly monodisperse glass beads having diameters of 0.5, 1.1, and 2.2 mm, with corresponding particle Reynolds numbers of 106, 373, and 990; particle volume fractions less than 0.003%; direct rates of dissipation of turbulence by particles less than 4%; and rates of turbulence generation sufficient to yield streamwise relative turbulence intensities of 0.2–1.5%. The major conclusions of the study are as follows:

1) The dissipation-weighted mixing rules of Eqs. (10–12) provided an effective way to generalize earlier correlations of the properties of the turbulent interwake region for monodisperse particle phases, reported in Ref. 7, to various binary mixtures of monodisperse particles studied during the present investigation. It is a straightforward matter to extend these relationships to polydisperse particle phases; therefore, this methodology provides a way to estimate the properties of the interwake region of practical dispersed multiphase flows involving polydisperse particle phases.

2) The turbulent interwake region produced by homogeneous flows of polydisperse particle phases was homogeneous and nearly isotropic with PDFs of streamwise and cross-stream velocities well approximated by Gaussian functions and with no property of the interwake region exhibiting a bimodal behavior that reflected the bimodal dispersed phases used to study the present flows.

3) The relative turbulence intensities of the turbulent interwake region could be correlated in the same manner for monodisperse and polydisperse particle phases following the approach of Ref. 7, based on an analogy with the known properties of isotropic grid-generated turbulence from Batchelor and Townsend.[9,10] This was done by scaling these properties, using mixing rules for binary dispersed phases, with mean particle spacings normalized by the particle-wake momentum diameter to yield a normalized dimensionless dissipation factor that is simply related to the streamwise and cross-stream relative turbulence intensities, as given by Eqs. (13).

4) Existing measurements of the turbulent interwake region for monodisperse and polydisperse particle phases showed that the turbulent interwake region exhibited small turbulence Reynolds numbers, $Re_\lambda < 3.5$ for present test conditions, and was in the final-decay period of isentropic turbulence as defined by Batchelor and Townsend,[9,10] where vortical regions fill the entire turbulent interwake region but are sparse, that is, where turbulence appears to involve disconnected turbulent spots when single-point measurements are observed.

5) Within the final-decay period, rates of dissipation are enhanced compared to conventional isotropic turbulence at large turbulence Reynolds numbers having similar values of L_u and $\bar{u}'$ (see Fig. 5). In addition, macroscale/microscale ratios (e.g., L_u/λ) decrease with increasing turbulence Reynolds numbers in the final-decay period as opposed to increasing with increasing turbulence Reynolds number, which is typical of conventional isotropic turbulence at large turbulence Reynolds numbers. Thus, flows in the final-decay period can exhibit a large range of scales even though their turbulence

Reynolds numbers are small. In addition, this behavior implies that turbulence in the final-decay period can have a large range of scales where effects of viscosity are small, yielding a $-\frac{5}{3}$ Kolmogorov-like, inertial-decay region of the energy spectra, for the same reasons that similar inertial-decay regions are observed for conventional turbulence at large turbulence Reynolds numbers.

Acknowledgments

This investigation was supported by the U.S. Air Force Office of Scientific Research, Grants F49620-99-1-0083 and F49620-02-1-0074, under the technical management of J. M. Tishkoff. Helpful discussions with W. J. A. Dahm are gratefully acknowledged. The U.S. Government is authorized to reproduce and distribute copies of the paper for governmental purposes notwithstanding any copyright notation thereon.

References

[1]Parthasarathy, R. N., and Faeth, G. M., "Turbulence Modulation in Homogeneous Dilute Particle-Laden Flows," *Journal of Fluid Mechanics*, Vol. 220, Pt. 2, 1990, pp. 485–514.

[2]Mizukami, M., Parthasarathy, R. N., and Faeth, G. M., "Particle-Generated Turbulence in Homogeneous Dilute Dispersed Flows," *International Journal of Multiphase Flow*, Vol. 18, No. 2, 1992, pp. 397–412.

[3]Wu, J.-S., and Faeth, G. M., "Sphere Wakes in Still Surroundings at Intermediate Reynolds Numbers," *AIAA Journal*, Vol. 31, No. 8, 1993, pp. 1448–1455.

[4]Wu, J.-S., and Faeth, G. M., "Sphere Wakes at Moderate Reynolds Numbers in a Turbulent Environment," *AIAA Journal*, Vol. 32, No. 3, 1994, pp. 535–541.

[5]Wu, J.-S., and Faeth, G. M., "Effects of Ambient Turbulence Intensity on Sphere Wakes at Intermediate Reynolds Numbers," *AIAA Journal*, Vol. 33, No. 1, 1995, pp. 171–173.

[6]Chen, J.-H., Wu, J.-S., and Faeth, G. M., "Turbulence Generation in Homogeneous Particle-Laden Flows," *AIAA Journal*, Vol. 38, No. 4, 2000, pp. 636–642.

[7]Chen, J.-H., and Faeth, G. M., "Interwake Turbulence Properties of Homogeneous Particle-Laden Flows," *AIAA Journal*, Vol. 38, No. 6, 2000, pp. 995–1001.

[8]Chen, J.-H., and Faeth, G. M., "Continuous-Phase Properties of Homogeneous Particle-Laden Turbulent Flows," *AIAA Journal*, Vol. 39, No. 1, 2001, pp. 180–183.

[9]Batchelor, G. K., and Townsend, A. A., "Decay of Isotropic Turbulence in the Initial Period," *Proceedings of the Royal Society of London*, Vol. 193A, No. 8, 1948, pp. 539–558.

[10]Batchelor, G. K., and Townsend, A. A., "Decay of Turbulence in the Final Period," *Proceedings of the Royal Society of London*, Vol. 194A, No. 8, 1948, pp. 527–543.

[11]Kistler, A. L., and Vrebalovich, T., "Grid Turbulence at Large Reynolds Numbers," *Journal of Fluid Mechanics*, Vol. 26, Pt. 1, 1966, pp. 37–47.

[12]Compte-Bellot, G., and Corrsin, S., "Simple Eulerian Time Correlation of Full- and Narrow-Band Velocity Signals in 'Grid-Generated' Isotropic Turbulence," *Journal of Fluid Mechanics*, Vol. 48, Pt. 2, 1971, pp. 273–337.

[13]Mohamed, M. S., and LaRue, J. C., "The Decay Power Law in Grid-Generated Turbulence," *Journal of Fluid Mechanics*, Vol. 219, Pt. 1, 1990, pp. 195–214.

[14]Tong, C., and Warhaft, Z., "On Passive Scalar Derivative Statistics in Grid Turbulence," *Physics of Fluids*, Vol. 6, No. 6, 1994, pp. 2165–2176.

[15]Mydlarski, L., and Warhaft, Z., "On the Onset of High-Reynolds-Number Grid-Generated Wind Tunnel Turbulence," *Journal of Fluid Mechanics*, Vol. 320, Pt. 2, 1996, pp. 331–368.

[16]Jiminez, J., Wray, A. A., Saffman, P. G., and Rogallo, R. S., "The Structure of Intense Vorticity in Isotropic Turbulence," *Journal of Fluid Mechanics*, Vol. 255, Pt. 1, 1993, pp. 65–90.

[17]Wang, L.-P., Chen, S., Brasseur, J. G., and Wyngaard, J. C., "Examination of Hypotheses in the Kolmogorov Refined Turbulence Theory Through High-Resolution Simulations. Part I Velocity Field," *Journal of Fluid Mechanics*, Vol. 309, Feb. 1996, pp. 113–156.

[18]Yeung, P. K., and Zhou, Y., "On the Universality of the Kolmogorov Constant in Numerical Simulation of Turbulence," *Physical Review E*, Vol. 18, No. 7, 1997, p. 1746.

[19]Cao, N., Chen, S., and Doolen, G. D., "Statistics and Structure of Pressure in Isotropic Turbulence," *Physics of Fluids*, Vol. 11, No. 8, 1999, pp. 2235–2250.

[20]Sreenivasan, K. R., "An Update on Energy Dissipation Rate in Isotropic Turbulence," *Physics of Fluids*, Vol. 10, No. 2, 1998, p. 529.

[21]Ling, S. C., and Huang, T. T., "Decay of Weak Turbulence," *Physics of Fluids*, Vol. 13, No. 12, 1970, pp. 2912–2924.

[22]Phillips, O. M., "The Final Period of Decay of Non-Homogeneous Turbulence," *Proceedings of the Cambridge Philosophical Society*, Vol. 52, Pt. 1, 1956, pp. 135–151.

[23]Chen, J.-H., "Turbulence Generation in Homogeneous Dilute Particle-Laden Flows," Ph.D. Dissertation, Dept. of Aerospace Engineering, Univ. of Michigan, Ann Arbor, MI, 1999.

[24]Buchhave, P., "The Measurement of Turbulence with the Burst-Type Laser Doppler Anemometer—Errors and Correction Methods," Ph.D. Dissertation, Dept. of Mechanical and Aerospace Engineering, State Univ. of New York, Buffalo, NY, 1979.

[25]Buchhave, P., George, W. K., and Lumley, J. L., "The Measurement of Turbulence with the Laser-Doppler Anemometer," *Annual Review of Fluid Mechanics*, Vol. 11, 1979, pp. 443–504.

[26]Hinze, J. O., *Turbulence*, 2nd ed., McGraw–Hill, New York, 1975, Chap. 3, pp. 65–67, 202–211, 496–519.

[27]Putnam, A. A., "Integrable Form of the Droplet Drag Coefficient," *ARS Journal*, Vol. 31, No. 10, 1961, pp. 1467, 1468.

[28]Batchelor, G. H., *The Theory of Homogeneous Turbulence*, Cambridge Univ. Press, Cambridge, England, U.K., 1953, pp. 163–173.

[29]Bennett, J. C., and Corrsin, S., "Small Reynolds Number Nearly Isotropic Turbulence in a Straight Duct and a Contraction," *Physics of Fluids*, Vol. 21, No. 12, 1978, pp. 2129–2140.

R. M. C. So
Associate Editor